Research Article

Lin Li*, Haofan Wang, and Jinfeng Ma

Prediction method of S-wave velocities in tight sandstone reservoirs – a case study of CO₂ geological storage area in Ordos Basin

Abstract: S-wave velocity, among the critical parameters essential for developing 3D/4D seismic forward models, is prominent. Variations in both P- and S-wave velocities result from changes in the formation pressure and fluid saturation inside reservoirs during CO₂ geological storage operations. This study, understanding the significant variety and uneven stress distributions of tight sandstone reservoirs in the Ordos Basin, begins with developing a predictive model for S-wave velocities. The model integrates the Digby and DEM models and takes into account the changes in the formation pressure and alterations in pore shapes. Data from petrophysical experiments are used to validate this model. By comparing the shear wave velocity prediction results under four pore shapes, spherical, needle-shaped, disc-shaped, and coin-shaped gaps, the dominant pore shape of this sedimentary facies belt was selected, and the pore shape of the target layer was identified as needle-shaped pores. The shear wave velocity prediction model for this area was then optimized. Moreover, by analyzing actual well logging data, the methodology is validated and it shows high accuracy when using the dominant pore shapes to predict the S-wave velocity. This study emphasizes how important it is to take geological factors into account when developing 3D/4D seismic petrophysical predication models of S-wave velocities specifically designed for tight sandstone reservoirs.

* **Corresponding author: Lin Li,** College of Urban and Environmental Sciences, Northwest University, Xi'an 710127, China; National & Local Joint Engineering Research Center of Carbon Capture and Storage Technology, Xi'an 710069, China; Shaanxi Key Laboratory for Neutral Technology, Xi'an 710069, China; Carbon Neutrality College (Yulin), Northwest University, Xi'an 710000, China, e-mail: lilin_hyg@163.com
Haofan Wang, Jinfeng Ma: Department of Geology, Northwest University, Xi'an 710069, China; National & Local Joint Engineering Research Center of Carbon Capture and Storage Technology, Xi'an 710069, China; Shaanxi Key Laboratory for Neutral Technology, Xi'an 710069, China; Carbon Neutrality College (Yulin), Northwest University, Xi'an 710000, China

1 Introduction

Reducing global greenhouse gas emissions and taking aggressive measures to address climate change are among the most serious issues facing the society today [1]. The central technology of Carbon capture, utilization, and storage (CCUS) emerges as a crucial mechanism for addressing these issues [2,3]. The use of four-dimensional (4D) seismic technology, which is essential for CO₂ storage site selection, underground storage safety monitoring, CO₂ distribution verification, and leak detection, is the core of effective CCUS projects [4,5]. Injection of CO₂ into subsurface reservoirs causes significant changes in key reservoir parameters, such as formation pressure and porosity. 4D seismic data subsequently exhibits observable responses to the changes. Therefore, it is crucial to take into account the dynamic variations in reservoir parameters when building 4D seismic forward models in order to improve the interpretation and inversion of such data.

P- and S-wave velocities are indispensable parameters in developing 4D seismic forward models. In recent years, geophysicists have come to realize the importance of the pressure as a critical factor in predicting the velocities of P- and S-waves as 4D seismic research in CO₂ geological storage continues to progress. Granular-medium rock-physics models, including the Hertz-Mindlin contact model [6], the Walton model [7], and the Digby model [8], incorporate the influence of the pressure on dry rock modulus. These models can be used to establish an effective relationship between the pressure and the velocities of P- and S-waves. Existing studies primarily center around the Hertz-Mindlin model [6]. Hossain et al. [9] developed a petrophysical model for North Sea Paleocene Green Sand using the Hertz-Mindlin model. Richesson and Sahimi [10] using the Hertz-Mindlin model, proposed a permeability forecasting model for porous media with variations in pore

size distribution under external pressures taken into account. Dvorkin and Nur [11] used the Hashin-Shtrikman bounds model [12] in combination with the Hertz-Mindlin model to predict acoustic velocities in highly porous rocks [13]. Weinzierl and Wiese [14] applied the Hertz-Mindlin model and the Biot-Gassmann equation to develop a petrophysical model and infer parameters, such as CO_2 saturation and pore pressure, by deep neural networks. Sayers and Dasgupta [15] studied unconsolidated sandstones in CO_2 injection regions, highlighted the limitations of the Hertz-Mindlin model and proposed a novel method to characterize granular contact properties via inversion. In response to the coordination number issue in the Hertz-Mindlin model, Makse et al. [16] used experimental data from empirical formulas for coordination numbers and the relationship between porosity and pressure in numerical simulations to validate the model. Garcia and Medina [17] confirmed the correlation between the coordination number, porosity, and hydro-static pressure, which verified the Hertz-Mindlin model. Zimmer et al. [18] effectively predicted the bulk modulus of glass beads based on empirical formulas of the coordination number, showing good agreement with the experimental data. Li and Ma [19,20] using both Hertz-Mindlin and Digby models, proposed a methodology to calculate the coordination number and build 4D seismic prediction models of P- and S-wave velocities.

Despite extensive research conducted by geophysicists, most existing models are developed for unconsolidated porous sandstone reservoirs. The Ordos Basin, China's second-largest sedimentary basin, has two CO_2 geological storage demonstration projects and also has multiple reservoir-seal combinations. Its geological structure is stable with minimal faults and fewest seismic activities, thus having a huge potential for CO_2 geological storage [21]. However, reservoirs in the Ordos Basin are tight sandstone reservoirs characterized by varied mineral compositions, complex pore structures, low porosity and permeability, and substantial heterogeneity. Given its critical role in determining the elastic properties of tight sandstones, the pore structure poses a challenge in this context [22–26]. Previous studies often used differential effective medium (DEM) models to develop prediction models of P- and S-wave velocities for tight sandstone reservoirs [27–30], considering the complex pore structure of tight reservoirs in the Ordos Basin.

In conclusion, granular contact models can be utilized to build 4D seismic prediction models of P- and S-wave velocities, but the models are ineffective for the complex pore structure of tight sandstone reservoirs. The DEM model can adequately explain the complex pore structure of tight sandstone reservoirs, but it is unsuitable for 4D seismic modeling as pressure effects are not included in the model. This study considers both factors and proposes an integrated approach that combines the granular contact model with the DEM model to develop prediction models of P- and S-wave velocities which change with the pressure and pore structures for tight sandstone reservoirs. The endeavor aims to provide theoretical support for the comprehensive and large-scale implementation of CO_2 geological storage in the Ordos Basin of China.

2 Theoretical foundation

2.1 Digby model

In 1981, Digby introduced a method to calculate the bulk modulus of dry rocks that varies with pressure, as shown in equations (1) and (2) [8].

$$K_{dry} = \frac{C_p(1 - \phi)\mu_{ma}b}{3\pi R(1 - v)}, \tag{1}$$

$$\mu_{dry} = \frac{C_p(1 - \phi)}{20\pi R}\left(\frac{4\mu_{ma}b}{1 - v} + \frac{12\mu_{ma}a}{2 - v}\right), \tag{2}$$

where b can be expressed as equation (3)

$$\frac{b}{R} = \left[d^2 + \left(\frac{a}{R}\right)^2\right]^{\frac{1}{2}}. \tag{3}$$

and d satisfies equation (1), refer equation (4)

$$d^3 + \frac{3}{2}\left(\frac{a}{R}\right)^2 d - \frac{3\pi(1 - v)p}{2C_p(1 - \phi)\mu_{ma}} = 0. \tag{4}$$

Based on Murphy's work, Li and Ma [20] proposed the calculation formula of the coordination number C as follows [31]:

$$C_p = W(11.759e^{1-\phi} - 12.748), \tag{5}$$

where K_{dry} and μ_{dry} represent the bulk modulus and shear modulus of dry rocks, respectively; v and μ_{ma}, respectively, denote the Poisson's ratio and shear modulus of rock matrix; ϕ is the porosity; C_p represents the coordination number; P is the differential pressure; a denotes the radius of the contact area before deformation, b signifies the radius of the contact area after deformation, and R represents the radius of the particle; W is the weighting coefficient.

2.2 Differential effective medium model

According to the theory of Differential effective medium (DEM), the elastic modulus of a biphasic composite is

obtained by simulating the gradual embedding of inclusions into solid mineral phases [32–34]. Within the DEM model, asymmetric relationships between the components that make up rocks enable the selection of different solid minerals as the primary phases. When there are multiple types or diverse shapes of inclusions, the effective modulus will rely not only on the final volume fractions of each component, but also significantly on the order of inclusion. Dry cavity can be simulated by setting the inclusions to zero.

Berryman [27] presented the expression of the DEM model for multi-phase medium mixtures with a system of differential equations, namely, the coupling of the effective bulk modulus K^* and the effective shear modulus μ^*, as shown in equations (6) and (7).

$$(1 - y)\frac{\mathrm{d}}{\mathrm{d}y}[K^*(y)] = (K_2 - K^*)P^{(*2)}(y), \quad (6)$$

$$(1 - y)\frac{\mathrm{d}}{\mathrm{d}y}[\mu^*(y)] = (\mu_2 - \mu^*)Q^{(*2)}(y). \quad (7)$$

The initial conditions are: $K^*(0) = K_1$ and $\mu^*(0) = \mu_1$, where K^* and μ^*, respectively, represent the DEM bulk modulus and the shear modulus, K_1 and μ_1 are the bulk modulus and the shear modulus of the initial dominant phase (Phase 1), respectively, K_2 and μ_2 denote the bulk modulus and the shear modulus of gradually introduced inclusions (Phase 2), respectively; y is the volume fraction of inclusions (Phase 2), typically representing rock porosity; $P^{(*2)}$ and $Q^{(*2)}$ are geometric factors for introducing inclusion Phase 2 against the background materials of the effective modulus K^* and μ^*. The shapes of inclusions include sphere, needle, disk, and penny cracks [35].

Since the DEM model simulates the properties of saturated rocks at high frequencies, the Gassmann equation [36] can be used to introduce fluid at low frequencies after the effective modulus of dry cavity is determined.

2.3 Digby-DEM model

The Digby model can be used to calculate the bulk modulus and the shear modulus of dry rocks that vary with the pressure. However, in the Digby model, influence of pore shapes on the bulk and the shear modulus of dry rocks is not considered. In this study, a petrophysical model was established which considered both pressure variations and diverse pore shapes by integrating the Digby model with the DEM model. The specific steps are outlined as follows:

(1) Based on the mineral composition and content of sandstone reservoir rocks, the Voigt-Reuss-Hill averaging model was used to calculate the bulk and the shear modulus of mineral particles.

(2) Substituting equation (5) in the Digby model, a Digby model was obtained, which contained the unknown variable W, namely, $K_{\text{Digby}}(W)$ and $\mu_{\text{Digby}}(W)$.

(3) Considering the complexity of pore shapes in sandstone reservoirs, especially in tight sandstone reservoirs, $K_{\text{Digby}}(W)$ and $\mu_{\text{Digby}}(W)$ were introduced into the DEM model as the initial dominant phase. Since cavities were added, K_2 and μ_2 were set to 0. As per equations (8) and (9), $P^{(*2)}$ and $Q^{(*2)}$ represented the geometric factors for introducing inclusion Phase 2 against the background materials of the effective modulus K^* and μ^*. These parameters, being related to pore shape, embodied the structural impact of pores on the modulus.

$$(1 - y)\frac{\mathrm{d}}{\mathrm{d}y}[K^*(y)] = (0 - K_{\text{Digby}}(W))P^{(*2)}(y), \quad (8)$$

$$(1 - y)\frac{\mathrm{d}}{\mathrm{d}y}[\mu^*(y)] = (0 - \mu_{\text{Digby}}(W))Q^{(*2)}(y). \quad (9)$$

(4) Based on the bulk modulus and the shear strain modulus of dry rocks that were obtained through DEM model simulations, fluid was injected into the cavities using the Gassmann equation [37]. The Gassmann equation was used to derive the bulk strain modulus $K_{\text{sat}}(W)$ of saturated rocks, and the shear strain modulus of saturated rocks equaled the shear modulus of the rock containing dry cavity rocks denoted as $\mu^*(W)$. However, due to the presence of the unknown variable W, directly obtaining the bulk and the shear modulus of dry and saturated rocks became impossible. The value of W can be computed with an iterative algorithm by measuring P-wave velocities, and ultimately the bulk modulus and the shear modulus of dry rocks can be obtained. This process involved the value determination of W with equations (10) and (11), followed by calculating the S-wave velocity with pressure and pore shape changes taken into account through equation (12). The specific iterative procedure is detailed in Figure 1.

$$V_{\text{ppredicted}} = \sqrt{\frac{K_{\text{sat}}(W) + \frac{4}{3}\mu*(W)}{\rho}}, \quad (10)$$

$$|V_{\text{ppredicted}} - V_{\text{pmeasured}}| \to 0, \quad (11)$$

$$V_{\text{spredicted}} = \sqrt{\frac{\mu*(W)}{\rho}}. \quad (12)$$

3 Case study

3.1 Geological background

The research area is in the western region of the Sulige Gas Field in the northern part of the Ordos Basin. Main gas
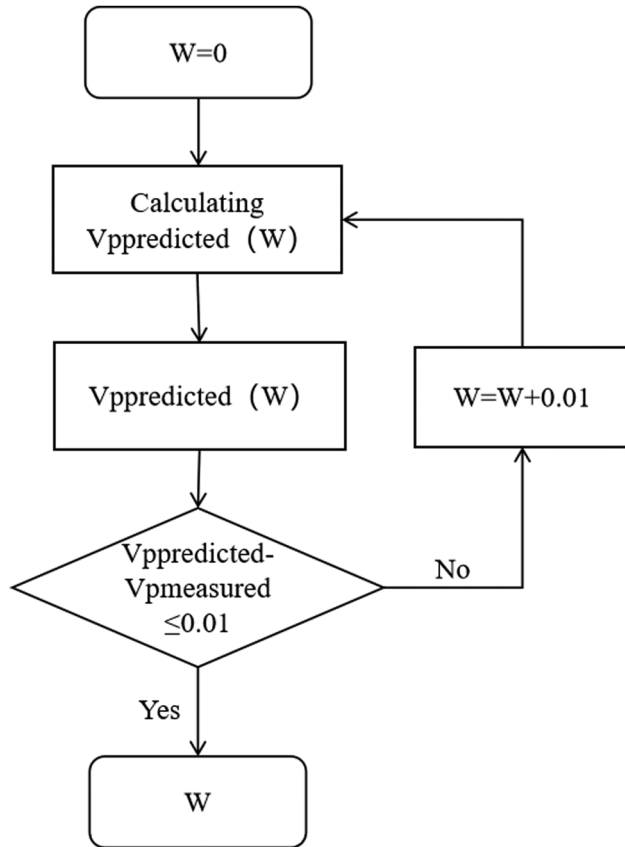
Figure 1: The weighted coefficient W obtained by iterative algorithm.

Figure 2: Map of sedimentary facies in the study area.

reservoirs include the Shihezi Formation Segment 8 and the Shanxi Formation Segment 1 with gas distribution being controlled by the Yi-Shaan slope, where there are mainly trap gas reservoirs with low porosity and low permeability litholog. The Shanxi Formation can be divided into two segments from the bottom to the top: Shan 2 and Shan 1. The Shan 2 segment contains delta plain deposits with delta front deposits appearing in the southern part, which comprises a sequence of coal-bearing clastic rock strata primarily composed of quartz sandstone interbedded with thin layers of siltstone, mudstone, and coal seams. The Shan 1 segment is primarily made up of delta plain deposits with mudstone and fine to medium-grained quartz sandstone. The Shihezi Formation Segment 8, however, contains delta plain deposits featuring light gray conglomeratic coarse sandstone, light gray medium-grained sandstone, and grayish-green interbedded mudstone and quartz sandstone. The upper part of Segment 8 is made up of shoreline deposits from shallow lakes and arid lakes, which are primarily composed of a sequence of red mudstone and sandy mudstone interbedded with thin layers of sandstone and siltstone (Figure 2). Thus, the Segment 8 of the Shihezi Formation and the Segment 1 of Shanxi Formation, which are

both characterized by low porosity and low permeability reservoirs, display complex pore structures and a variety of mineral compositions (Figure 3).

3.2 Petrophysical experiments

Wang [38] conducted ultrasonic petrophysical experiments using 51 rock samples from the Sulige Gas Field in the Ordos Basin to obtain elastic parameters, such as P- and S-wave velocities and density at specific pressures. The results can validate the methodology presented in this study. In this study, data from tests on five cores of four wells (Su4, Su5, Su8, and Su10) were used to study a predictive method for S-wave velocities in tight sandstones. The five cores were taken from the Shihezi and Shanxi Formations, respectively, with an experimental confining pressure of 29 MPa and a temperature of 105°C. On the basis of the DEM-Digby model, this study simulated four cases in which the pore shape was sphere, needle, disk, and penny cracks, and predictions for S-wave velocities were conducted, which were represented by V_{S1}, V_{S2}, V_{S3}, and V_{S4}, respectively, in the following paragraphs. The measured data and predicted results are shown in Table 1 and Figure 4.

Figure 4 shows the petrophysical test results and the S-wave velocities predicted by the Digby-DEM model, in
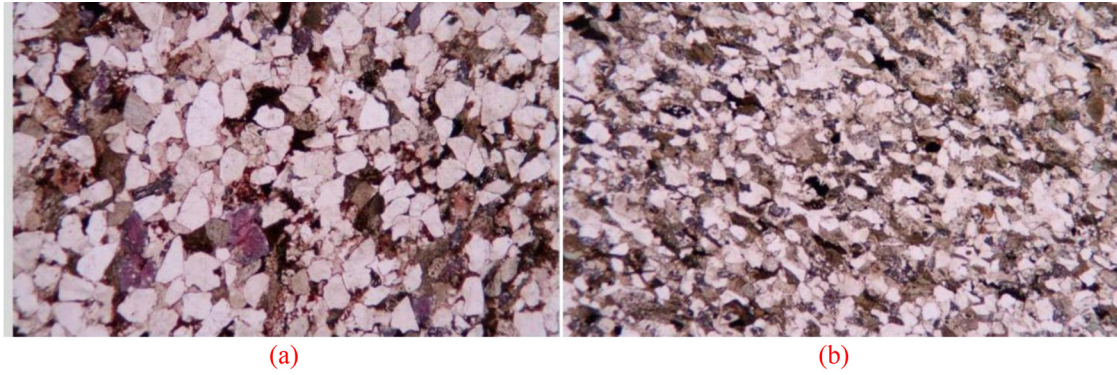
Figure 3: Pore structure characteristics of reservoirs in the Sulige Gas Field. (a) Pore structure characteristics of He 8. (b) Pore structure characteristics of Shan 1.

Table 1: Petrophysical test results and predictions

Well no.	Layers	Porosity (%)	Density (g/cm³)	Measured P-wave velocity V_p (km/s)	Measured S-wave velocity V_p (km/s)	Predicted S-wave velocity V_{S1} (km/s)	Predicted S-wave velocity V_{S2} (km/s)	Predicted S-wave velocity V_{S3} (km/s)	Predicted S-wave velocity V_{S4} (km/s)
Su 4	Shihezi Formation	6.99	2.49	4.961	3.011	2.910	2.962	3.059	2.761
Su 8	Shihezi Formation	4.98	2.57	4.659	2.817	2.718	2.728	2.911	2.702
Su 5	Shihezi Formation	3.81	2.58	5.234	3.157	3.048	3.049	2.757	2.757
Su 5	Shanxi Formation	4.96	2.55	4.780	2.889	2.783	2.823	3.058	2.761
Su10	Shanxi Formation	5.53	2.577	5.174	3.133	3.026	3.067	3.203	2.99

which the stars represent the measured S-wave velocities, the circles represent the predicted S-wave velocities. The colors of red, yellow, blue, and green correspond to the S-wave velocities under the four pore shapes, i.e., sphere, needle, disk, and penny cracks, respectively. The average errors with the measured S-wave velocities are 3.48, 2.52, 5.13, and 6.81%, respectively, for the respective conditions.

3.3 Verification of actual logging data

Using the methodology given in Section 2.3 of this study, S-wave velocities of Well Su 11, Well Su 51, and Well Su 130 in the Sulige Gas Field were predicted. The well location maps of the three wells are shown in Figure 2. Similar to Section 3.2, this study presented the predicted S-wave velocities for four pore shapes. For comparison, the Digby model was
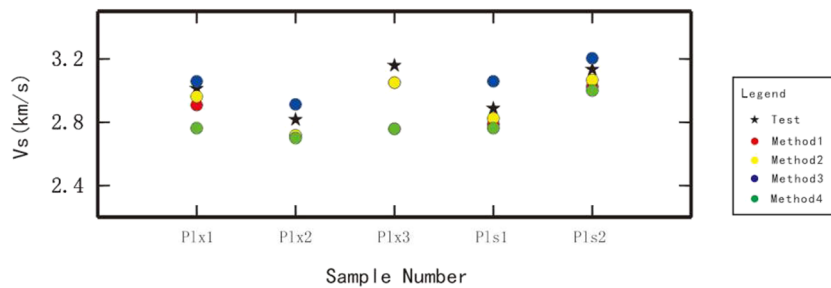
Figure 4: A Comparison of petrophysical test results and predicted results.

(a)

(b)

(c)
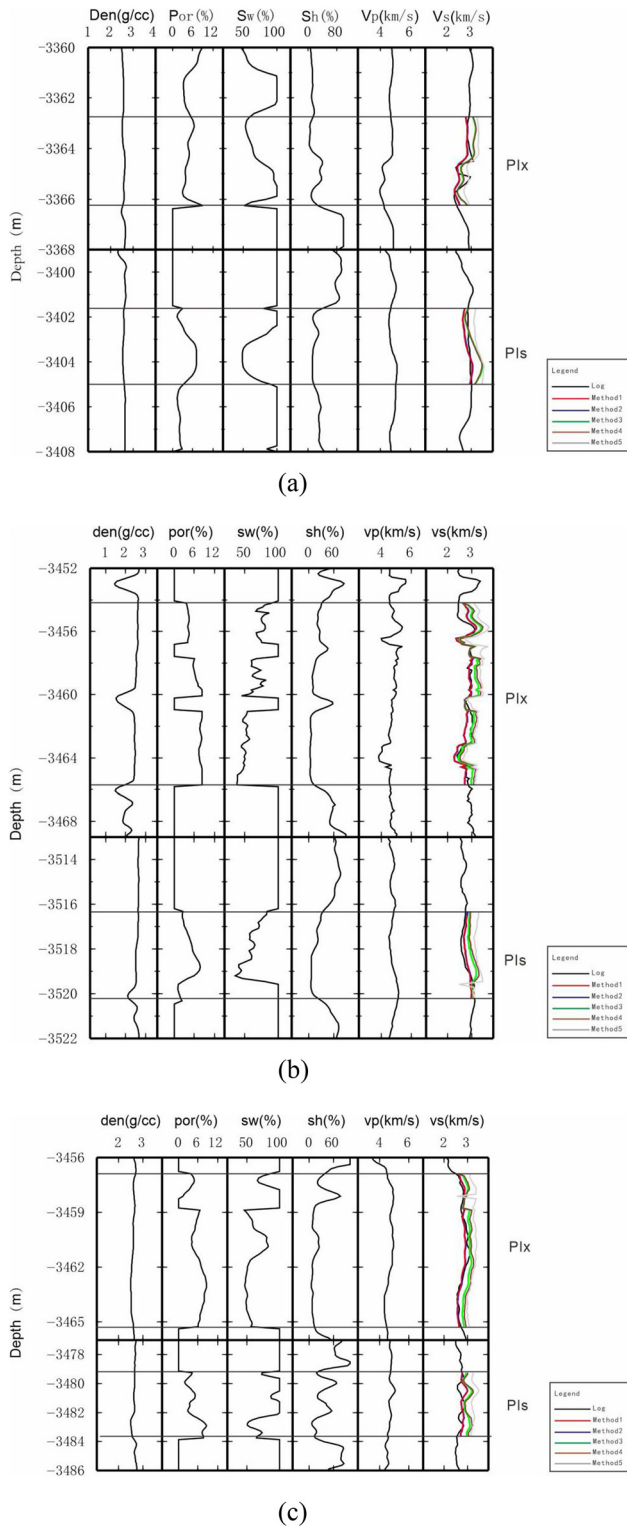
Figure 5: The logging results of the three wells in the Sulige Gas Field and a comparison between the measured and the predicted S-wave velocities. From left to right, there are the parameters of density, porosity, water saturation, clay content, and S-wave velocities. In the figure of S-wave velocities, the black line represents the actual measured S-wave velocities of the wells, while methods 1–4, respectively, correspond to predicted S-wave velocities based on the Digby-DEM model of simulated pore shapes of sphere, needle, disk, and coin slit. Method 5 is the directly predicted S-wave velocities by the Digby model. (a) Comparison between the measured and the predicted S-wave velocities for Well Su 11. (b) Comparison between the measured and the predicted S-wave velocities for Well Su 51. (c) Comparison between the measured and the predicted S-wave velocities for Well Su 130.

also used to directly predict the S-wave velocities in this area. The results are shown in Figure 5.

Given that the target layers of the Sulige Gas Field consist of Shihezi Segment 8 and Shanxi Segement 1, S-wave velocity predictions for both segments were conducted in this study. Table 2 displays the average errors between the S-wave velocities predicted by the five methods mentioned above and the measured S-wave velocities of the three wells.

4 Discussion

Many geophysicists have studied the prediction of P-wave velocity in low-permeability reservoirs in the Ordos Basin. In these studies, the complex pore structure of low-permeability reservoirs has been taken into account [30]. They referred to the elliptical pore models established for conventional sandstone reservoirs [39] and carbonate reservoirs [40], and constructed a rock physics model for tight sandstone. These models provide basic data for "sweet spot" prediction, amplitude variation with offset forward and inverse of tight sandstone.

In this study, Figure 2 shows the sedimentary plain distribution of Shihezi Segment 8 in the western part of the Sulige Gas Field in the Ordos Basin. By overlaying the well location map of the study area, the sedimentary facies associated with each well can be determined. River channel deposits, transitional zones, and floodplain deposits are examples of the known sedimentary facies types. Well Su 11 and Well Su 51 are taken as river channel deposits, while Well Su 130 is in the transitional zone and closely resembles river channel deposits in reality. After analyzing the results of petrophysical tests and the really well logging data, the average errors for the sphere and the needle models in the Digby-DEM model are found to be smaller. From comparing the needle and sphere models, it is evident that the average error of the needle model in the petrophysical well logging data is typically smaller than that of the sphere model. Furthermore, the average error of the sphere model in Shihezi Segment 8 is bigger than that of the needle model based on the really well logging data. However, predicted results for Wells Su 51 and Well Su 130 in Shanxi Segment 1 show that the average error of the sphere model

Table 2: Comparison of average errors

Well no.	Layers	Average error of sphere model (%)	Average error of needle model (%)	Average error of disk model (%)	Average error of coin slit fissure model (%)	Average error of Digby model (%)
Well Su 11	Shihezi Segment 8	5.75	5.54	6.44	6.33	10.54
	Shanxi Segment 1	3.91	3.83	7.62	7.34	12.77
Well Su 51	Shihezi Segment 8	5.13	5.05	6.43	8.78	12.10
	Shanxi Segment 1	3.39	3.55	8.39	10.40	16.10
Well Su 130	Shihezi Segment 8	3.79	3.68	6.01	8.15	15.20
	Shanxi Segment 1	4.77	4.90	11.8	5.11	15.4

is smaller than that of the needle model. In Well Su 11, the error of the needle model is slightly smaller than that of the sphere model. In general, the differences are not very noticeable. This suggests that the sedimentary facies zone is more suitable for the needle model and can be applied to other wells within the same sedimentary facies zone based on petrophysical predictions.

In the well logging data, the Digby model is also used in the study to directly predict S-wave velocity, and its average error exceeds 10%. When the Digby model is combined with the DEM model to predict the S-wave velocities in this area, the error is greatly reduced, indicating that in tight sandstone reservoirs, the prediction model of S-wave velocities solely considering pressure changes cannot meet the actual situation. It is necessary to establish a more realistic petrophysical model that takes into account both pressure changes and pore shape variations.

Through the research in this work, it can be found that when establishing a rock physics model for predicting shear wave velocity with pressure variation, pore shape is also one of the factors that must be considered, and the selection of pore shape is related to the sedimentary facies zone in which the area is located. Therefore, in practical applications, rock physics experiments need to be conducted first. By combining rock physics experiments with rock physics modeling, the pore shape of the study area can be determined, and then the shear wave velocity of the entire study area can be predicted.

5 Conclusion

This study analyzed the complex pore shapes in the tight sandstone reservoirs of the Sulige Gas Field, and a Digby-DEM model that incorporated both pressure factors and pore shapes in the predication of S-wave velocities was proposed. Through the validation of this method with petrophysical test results and well logging data in the area, the following conclusions are drawn:

(1) Conventional granular contact models that only consider pressure changes cannot be directly applied to tight sandstone reservoirs, and a rock physics model that takes in account the pore shapes is necessary as it is more in line with the complex pores in tight sandstone reservoirs.

(2) The pore shapes of the Digby-DEM model established in this study can be confirmed by using petrophysical test results of the same sedimentary facies zone and the same stratigraphic level. The confirmation of pore shapes can further enhance the accuracy of S-wave

velocity predictions during well logging, with most of the average errors being under 5%.

The Digby-DEM model, which considers both the pressure changes and the complex pore shapes in tight sandstone reservoirs, can predict P- and S-wave velocities under different pressures for 4D seismic forward modeling. This model can provide theoretical support for the widespread deployment of 4D seismic monitoring of CO_2 geological sequestration.

Author contributions: Li Lin was responsible for completing the methods and writing the paper, while Wang Haofan was responsible for the figures and tables in the paper. Ma Jinfeng was responsible for proofreading the paper.

Conflict of interest: Authors state no conflict of interest.

References

[1] IPCC. Climate Change 2022: Mitigation of Climate Change: Contribution of Working Group III to the Sixth Assessment Report of the Intergovernmental Panel on Climate Change. Cambridge, UK: Cambridge University Press; 2022.

[2] IEA (International Energy Agency). Energy technology perspectives 2017. Paris: OECD/IEA; 2017. p. 3–8.

[3] IEA (International Energy Agency). CCUS in clean energy transitions. Paris: OECD/IEA; 2020. p. 2–6.

[4] White DJ. Monitoring CO_2 storage during EOR at the Weyburn-Midale field. Lead Edge. 2009;28(7):838–42.

[5] Chadwick RA, Williams GA, Williams JDO, Noy DJ. Measuring pressure performance of a large saline aquifer during industrial-scale CO_2 injection: The Utsira Sand, Norwegian North Sea. Int J Greenh Gas Control. 2012;10:374–88.

[6] Mindlin RD. Compliance of elastic bodied in contact. J Appl Mechaics. 1949;16:259–68.

[7] Walton K. The effective elastic moduli of a random pack of spheres. J Mech Phys Solids. 1987;35:213–26.

[8] Digby PJ. The effective elastic moduli of porous granular rocks. J Appl Mech Technical Phys. 1981;48:803–8.

[9] Hossain Z, Mukerji T, Dvorkin J, Fabricius IL. Rock physics model of glauconitic greensand from the North Sea. Geophysics. 2011;76(6):199–209.

[10] Richesson S, Sahimi M. Hertz-Mindlin theory of contacting grains and the effective-medium approximation for the permeability of deforming porous media. Geophys Res Lett. 2019;46(14):8039–45.

[11] Dvorkin J, Nur A. Elasticity of high-porosity sandstones: Theory for two North Sea datasets. Geophysics. 1996;61:1363–70.

[12] Mavko G, Mukerji T, Dvorkin J. The rock physics handbook. Cambridge, UK: Cambridge University Press; 2020.

[13] Hashin Z, Shtrikman S. A variational approach to the elastic behavior of multiphase materials. J Mech Phys Solids. 1963;11(2):127–40.

[14] Weinzierl W, Wiese B. Deep learning a poroelastic rock-physics model for pressure and saturation discrimination. Geophysics. 2021;86(1):53–66.

[15] Sayers CM, Dasgupta S. Elastic properties of unconsolidated sandstones of interest for carbon storage. Geophys Prospect. 2024;72(2):617–32.

[16] Makse HA, Gland N, Johnson DL, Schwartz L. Granular packings: Nonlinear elasticity, sound propagation, and collective relaxation dynamics. Phys Rev E. 2004;70(6):061302.

[17] Garcia X, Medina E. Hysteresis effects studied by numerical simulations: cyclic loading-unloading of a realistic sand model. Geophysics. 2006;71:F13–20.

[18] Zimmer MA, Prasad M, Mavko G, Nur A. Seismic velocities of unconsolidated sands: part 1 pressure trends from 0.1 to 20 MPa. Geophysics. 2007;72:E1–13.

[19] Li L, Ma J. Study of shear wave velocity prediction during CO_2-EOR and sequestration in Gao 89 area of Shengli Oilfield. Appl Geophysics. 2017;14(3):372–80.

[20] Li L, Ma JF. The influence of pore system change during CO_2 storage on 4D seismic interpretation. Oil Gas Sci Technol. 2019;74(5):1–14.

[21] Ren XK, Cui YJ, Bu XP, Tan YJ, Zhang JQ. Analysis of CO_2 geological storage potential in Ordos Basin. Res Approach. 2010;32(1):29–32.

[22] Ba J, Du QZ, Carcione JM, Zhao H, Muller T. Seismic exploration of hydrocarbons in heterogeneous reservoirs: New theories, methods and applications. London: Elsevier Science; 2014. p. 978-0-12-420151-4.

[23] Chen YG, He YH, Wang C, Ge X, Ma F, Meng W, et al. Genesis and accumulation patterns of unconventional oil reservoir in Member 8 of Triassic Yanchang Formation: a case study of the western Ganquan area, southeastern Ordos Basin. Acta Petrolei Sin. 2021;42(10):1270–86.

[24] Fu ST, Jin ZJ, Fu JH, Li S, Yang W. Transformation of understanding from tight oil to shale oil in the Member 7 of Yanchang Formation in Ordos Basin and its significance of exploration and development. Acta Petrolei Sin. 2021;42(5):561–9.

[25] Yin XY, Liu XX, Cao DP. Elastic parameters calculation for tight sand reservoir based on Biotconsistent theory. Geophys Prospect Pet. 2013;52(5):445–51.

[26] Wang SW, Wang YB, Zheng YK, Chang X, Li J, Zeng R. Comparison of geological models for the simulation of CO_2 migration: a case study in Ordos, China. Greenh Gases: Sci Technol. 2021;11(2):277–96.

[27] Berryman JG. Single-scattering approximations for coefficients in Biot's equations of poroelasticity. J Acoust Soc Am. 1992;91(2):551–71.

[28] Huang XR, Huang JP, Li ZC. Anisotropic seismic rock physics model of tight oil sandstone based on double-porosity theory. Acta Petrolei Sin. 2015;36(10):1248–59.

[29] Tan W, Ba J, Mvller T. Rock physics model of tight oil siltstone for seismic prediction of brittleness. Geophys Prospect. 2020;68:1554–74.

[30] Liu ZS, Wang KN, Bao QZ, Li Z. Physics S-wave velocity in tight sandstone reservoir: a case study of Yanchang Formation in Ordos Basin. Acta Petrolei Sin. 2022;43(9):1284–94.

[31] Murphy WF. Effects of microstructure and pore fluids on the acoustic properties of granular sedimentary materials. Palp Alto: Stanford University; 1982.

[32] Cleary MP, Chen IW, Lee SM. Self-consistent techniques for heterogeneous media. J Eng Mech Div. 1980;106(5): 861–87.

[33] Norris AN. A differential scheme for the effective moduli of composites. Mech Mater. 1985;4(1):1–16.

[34] Zimmerman RW. Compressibility of sandstones. New York: Elsevier; 1991. p. 173.

[35] Berryman JG. Mixture theories for rock properties. Washington: American Geophysical Union; 1995. p. 205–28.

[36] Mavko G, Mukerji T. Bounds on low-frequency seismic velocities in partially saturated rocks. Geophysics. 1998;63(3):918–24.

[37] Gassmann F. Elastic waves through a packing of spheres. Geophysics. 1951;16(4):673–85.

[38] Wang DX. A study on the rock physics model of gas reservoirs in tight sandstone. Chin J Geophys (in Chinese). 2016;59(12):4603–22.

[39] Xu SY, White RE. A new velocity model for clay-sand mixtures. Geophys Prospect. 1995;43(1):91–118.

[40] Zhang GZ, Li CC, Yin XY, Zhang J. A shear velocity estimation method for carbonate rocks based on the improved Xu-White model. Oil Geophys Prospect. 2012;47(5):717–22.